# CXR-Net: A Multitask Deep Learning Network for Explainable and Accurate Diagnosis of COVID-19 Pneumonia from Chest X-ray Images

Xin Zhang, Liangxiu Han*, Tam Sobeih, Lianghao Han, Nina Dempsey, Symeon Lechareas, Ascanio Tridente, Haoming Chen, Stephen White, Daoqiang Zhang

*Abstract*—Accurate and rapid detection of COVID-19 pneumonia is crucial for optimal patient treatment. Chest X-Ray (CXR) is the first-line imaging technique for COVID-19 pneumonia diagnosis as it is fast, cheap and easily accessible. Currently, many deep learning (DL) models have been proposed to detect COVID-19 pneumonia from CXR images. Unfortunately, these deep classifiers lack the transparency in interpreting findings, which may limit their applications in clinical practice. The existing explanation methods produce either too noisy or imprecise results, and hence are unsuitable for diagnostic purposes. In this work, we propose a novel explainable CXR deep neural Network (CXR-Net) for accurate COVID-19 pneumonia detection with an enhanced pixel-level visual explanation using CXR images. An Encoder-Decoder-Encoder architecture is proposed, in which an extra encoder is added after the encoder-decoder structure to ensure the model can be trained on category samples. The method has been evaluated on real world CXR datasets from both public and private sources, including healthy, bacterial pneumonia, viral pneumonia and COVID-19 pneumonia cases. The results demonstrate that the proposed method can achieve a satisfactory accuracy and provide fine-resolution activation maps for visual explanation in the lung disease detection. The Average Accuracy, Sensitivity, Specificity, PPV and F1-score of models in the COVID-19 pneumonia detection reach 0.992, 0.998, 0.985 and 0.989, respectively. Compared to current state-of-the-art visual explanation methods, the proposed method can provide more detailed, high-resolution, visual explanation for the classification results. It can be deployed in various computing environments, including cloud, CPU and GPU environments. It has a great potential to be used in clinical practice for COVID-19 pneumonia diagnosis.

Xin Zhang, Liangxiu Han, Tam Sobeih are with the Department of Computing, and Mathematics, Manchester Metropolitan University, Manchester M15GD, UK (e-mail: x.zhang@mmu.ac.uk; l.han@mmu.ac.uk;T.Sobeih@mmu.ac.uk)

Lianghao Han is with the Department of Computer Science, Brunel University, Uxbridge UB8 3PH, UK (e-mail:lianghao.han@brunel.ac.uk)

Nina Dempsey is with the Department of Life Sciences, Manchester Metropolitan University, Manchester M1 5GD, UK (e-mail:n.dempsey-hibbert@mmu.ac.uk)

Symeon Lechareas is with the Radiology, Whiston Hospital, St Helens and Knowsley Teaching Hospitals NHS Trust, Warrington Road, Prescot L35 5DR, UK (e-mail:symeon.lechareas@rlbuht.nhs.uk)

Ascanio Tridente is with the Intensive Care Unit, Whiston Hospital, St Helens and Knowsley Teaching Hospitals NHS Trust, Warrington Road, Prescot L35 5DR, UK (e-mail:Ascanio.Tridente@sthk.nhs.uk)

Haoming Chen is with the Computer Science and Artificial Intelligence,University of Sheffield, Sheffield S1 4DP, UK (e-mail:hchen78@sheffield.ac.uk)

Stephen White is with the Cardiovascular Pathology, Manchester Metropolitan University, Manchester M1 5GD, UK (e-mail:stephen.white@mmu.ac.uk)

Daoqiang Zhang is with the College of Computer Science and Technology, Nanjing University of Aeronautics and Astronautics, Nanjing 210016, China (e-mail: dqzhang@nuaa.edu.cn)

Corresponding author*: L. Han (e-mail: l.han@mmu.ac.uk)

*Index Terms*—CXR imaging; Lung Disease; COVID-19; Deep Learning; Model Explanation/Explainable Artificial Intelligence

## I. INTRODUCTION

TABLE I
LIST OF ABBREVIATIONS AND ACRONYMS USED IN THIS PAPER.

| Abbreviation | Definition | Abbreviation | Definition |
|---|---|---|---|
| ACC | Average Accuracy | GAN | Generative Adversarial Network |
| AI | Artificial Intelligence | GGO | Ground-Glass Opacity |
| AUC | Area Under the Curve | LIME | Local Interpretable Model-Agnostic Explanations |
| CAM | Classification Activation Map | LR | Learning Rate |
| CLAHE | Contrast Limited Adaptive Histogram Equalization | PPC | Probability Perturbation Curve |
| CNN | Convolutional Neural Network | PPV | Positive Predictive Value |
| COVID-19 | COronaVIrus Disease 2019 | ROC | Receiver Operating Characteristics |
| CT | Computer Tomography | ROI | Regions Of Interest |
| CXR | Chest X-Ray | RT-PCR | Reverse Transcription Polymerase Chain Reaction |
| DL | Deep Learning | SARS-CoV-2 | Severe Acute Respiratory Syndrome Coronavirus 2 |
| DSC | Dice Score Coefficient | TN | True Negative |
| FN | False Negative | TP | True Positive |
| FP | False Positive | XGBoost | Extreme Gradient Boosting |

Since December 2019, the world has been experiencing a global pandemic from the emergence and spread of the potentially fatal COVID-19 (COronaVIrus Disease 2019) caused by severe acute respiratory syndrome coronavirus 2 (SARS-CoV-2) [1]. To optimise the management of this disease, accurate and rapid diagnosis is essential.

Reverse transcription Polymerase chain reaction (RT-PCR) has been recognised as an important method for the diagnosis of SARS-CoV-2 [2], [3]. However, the limited availability of test kits could severely delay the diagnosis of COVID patients who may need immediate quarantine for transmission prevention. Combining with clinical signs and symptoms, medical imaging is another widely used approach for the diagnosis of COVID-19. CXR and Computer tomography (CT) are two appropriate imaging modalities [4], [5], [6], [7]. The COVID-19 pneumonia imaging characteristics on CT include extensive consolidation, ground-glass opacity (GGO), symptom of acute pulmonary injury, lung consolidation, lung fibrosis, bilateral blotchy shadows, multiple lesions and wacky pavement pattern etc.[8], [9]. Compared to CT, CXR has some advantages: it is faster, cheaper and more widely accessible, and has a low level of radiation exposure to patients [5]. However, CXR has poor sensitivity and CXR-based medical image analyses have shown high positive predictive values for the detection of COVID-19 related pulmonary opacity. Therefore, developing fast and easily interpretable CXR analysis techniques are extremely useful for timely, trustful and reliable diagnosis of COVID-19.

Over the past several years, deep learning (DL) methods have shown enormous potential in medical imaging analyses for disease detection. With increasing publicly available CXR

images, various deep learning-based methods have been extensively used in the diagnosis of lung related diseases including COVID-19 [10], [11]. These methods can be broadly divided into two related categories: Organ area segmentation [12], [13], [14], [15] and Lung disease diagnosis (classification) [16], [17], [18].

Organ area segmentation is a useful way to improve the accuracy of diagnostic models through reducing the effect of disease-unrelated information in a CXR image. However, it usually requires manual annotation from clinical experts, which is labour-intensive and costly. With the help of deep learning-based semantic segmentation algorithms, automatic annotation of specific organs in medical images can be achieved. In [13] and [14], the authors used deep learning-based segmentation methods for organs and lesions recognition.

Deep learning models have also been used extensively for the diagnosis of lung diseases through image classification. In [19], a convolutional neural network called COVID-Net was designed to detect COVID-19 using CXR images consisting of only 358 COVID cases and 13,445 non-COVID cases, with an accuracy of 92.6%. Almost all the most commonly used deep learning-based classifiers, such as AlexNet, DenseNet, ResNet etc., have been used for the lung disease classification on CXR images and have achieved a reasonably high accuracy [10], [20]. In [21], a deep learning-based method using deep feature extraction and eXtreme Gradient Boosting (XGBoost) [22] was developed for identifying COVID-19 patients. The proposed method achieved an accuracy of 98.71% and F1-score of 99.25% in COVID-19 diagnosis. However, these deep learning models are black box models which are not straightforwardly explainable to clinicians, leading to a limited understanding of predictions. Some researchers have tried to use existing artificial intelligence (AI) explanation methods to interpret the image classification results of patients based on CXR images [23], [24], [25], [26]. Unfortunately, the results obtained in a pixel level from these methods were either too noisy or imprecise with low resolution, and hence are not suitable for medical diagnostic purposes.

To address the aforementioned limitations, particularly with respect to understanding the classification results, the current work presents an explainable classification model for COVID-19 pneumonia identification with enhanced visualisation of feature representations, named CXR-Net. The contributions of this paper include:

1) From a clinical perspective, a novel deep learning-based COVID-19 pneumonia diagnosis tool has been designed and implemented, allowing for both accurate lung disease classification and pixel-level visual explanation. This tool can be used to assist radiologists in screening patients with suspected COVID-19, thereby reducing the waiting time for clinical decisions.
2) From a methodological perspective, a novel Encoder-Decoder-Encoder based multitask (classification and explanation) deep learning model has been designed. It consists of two jointly trained encoders for classification. The first one is used to learn the features of original CXR images and the second one is used to learn the features

of the representation image generated from the decoder. The representation image between the two encoders acts as a proxy to visualise the most relevant infected areas for COVID-19 pneumonia diagnosis.
3) The proposed method has been validated against both publicly available and the private hospital datasets, which demonstrates the model generalisability and robustness for Lung-related and COVID-19 diseases.

The remainder of this paper is organised as follows: Section II reviews related work. Section III describes the datasets and methods; Section IV presents the experiment design and results; and Section V concludes the work.

## II. RELATED WORK

In this section, we review two types of deep learning-based applications related to our work, including Organ area segmentation and Lung disease diagnosis (classification).

### A. Organ Area Segmentation

Extracting different areas and lesions from CXR images can provide doctors with more focused relevant information in diagnosing and quantifying lung diseases [27]. Deep learning-based image segmentation methods have been used to detect the abnormalities in CXR images. In [13], Gal et al. proposed an attention U-Net based adversarial architecture for lung areas segmentation using CXR images of COVID and Non-COVID patients. The method performed well on the CXR images of unknown datasets with various patient characteristics, attaining a DSC (Dice Score Coefficient) accuracy of 97.5%. In [28], Vision Pro Deep Learning (A Deep Learning Software from COGNEXs), was used to classify and segment the regions of diseases and lungs from CXR datasets. The results were compared with various state-of-the-art Deep Learning models from the open-source community and achieved an F-score of 95.3% . In [14], Saeedizadeh et al. proposed a deep learning framework for organ and abnormal area segmentation. The popular U-Net architecture through adding a connectivity to promote regularisation was used in their segmentation model. The trained model was able to achieve a high accuracy in detecting COVID-19.

### B. Lung Disease Diagnosis

In recent years, deep learning approaches have been increasingly used for lung disease diagnosis based on CXR images. Pranav Rajpurkar et al. [20] developed a 121-layer DenseNet model [29], called CheXNeXt. They used frontal view chest radiographs to determine the presence of fourteen distinct thoracic diseases, such as pneumonia, pleural effusion, pulmonary masses and nodules etc. The model was trained and validated on the "ChestX-ray8" dataset [30], a public repository of Chest X-ray images including 108,948 frontal view X-Ray images with eight lung disease labels (Atelectasis, Cardiomegaly, Effusion, Infiltration, Mass, Nodule, Pneumonia and Pneumothorax). Ivo M. Baltruschat et al. [31] used the same datasets to investigate the depth sensitivity of deep learning models on lung disease classification by testing

ResNet models [32] with three different depths (layers), 34, 50 and 101.

The deep learning-based classifiers have also been used for the diagnosis of COVID-19. There are two types of methods for COVID-19 detection, transfer learning/fine-tuning and novel architectures. Transfer learning/fine-tuning is a technique for initialising a model with the weights of a pre-trained model instead of using random values. This approach is usually based on existing model structures and uses the weights pre-trained on a large amount of more general data. Transfer learning/fine-tuning normally performs well with a limited dataset related to more specific problems in the domain of interests. In [33], [34], [35], [36], various classification architectures, including AlexNet [37], VGG [38], ResNet [32], Inception [39] and DenseNet [29], were selected for a comparative study of COVID-19 diagnosis. The weights of models pre-trained on ImageNet datasets were transferred for model initialisation. A high diagnostic accuracy of COVID-19 (Acc >90%) was achieved in their study on public CXR datasets. This outstanding performance showed that the deep learning-based classifiers can accurately and effectively detect COVID-19, thereby providing potential benefits for improving patient care in clinical practice. Narin et al. [35] used CXR images of COVID-19 and non-COVID patients to fine-tune a ResNet-50 deep learning model for COVID-19 automatic classification, and achieved an accuracy of 98%. Zhang et al. [26] fine-tuned a deep learning model to distinguish between COVID-19 patients and pneumonia patients from a CXR image dataset of 70 patients diagnosed with COVID-19 and other pneumonia. The proposed deep learning model could reach a sensitivity of 90% in the detection of COVID-19 pneumonia and a specificity of 87.84% in the detection of non-COVID-19 pneumonia. However, existing pre-trained models were trained on general-purpose conventional images. CXR images have their own range of values and spatial features. Transfer learning/fine tune from generalised pre-trained models might introduce false biases [40].

Another approach to using deep learning for COVID diagnosis is to develop novel architectures for medical image data. Ozturk et al. [41] developed a deep learning model, called DarkCovidNet, to perform single and multiple category classification on CXR images of COVID-19 and other pneumonia patients. The whole dataset included 127 COVID-19, 500 non-infected and 500 other infectious pathogens pneumonia cases. The model produced an accuracy of 98% for binary classification and 87.02% for multi-category classification. In [42], a capsule network-based framework (COVID-CAPS) was designed to detect COVID infection from CXR and CT images. One benefit of using a capsule network is that it performs well with limited data. In [43], a lightweight deep neural network was designed to accurately detect COVID-19, bacterial pneumonia and normal cases from CXR images. In that work, a generative adversarial network (GAN) was trained to generate high quality COVID-19 images for model training in order to solve the problem of insufficient training data. Table. II shows the summary of the related work on the COVID-19 diagnosis based on the deep learning approaches.

Due to the existence of multiple non-linear structures in

TABLE II
THE SUMMARY OF RELATED WORK ON COVID-19 DIAGNOSIS BASED ON DEEP LEARNING APPROACHES.

| References | Categories | Deep Learning Algorithms |
|---|---|---|
| [33] | | VGG19, MobileNet v2, Inception, Xception, Inception ResNet v2 |
| [34] | | ResNet, Inception-v3, Inception ResNet-v2, DenseNet169, NASNetLarge |
| [35] | Transfer learning | ResNet50, ResNet101, ResNet152, InceptionV3 and Inception-ResNetV2 |
| [36] | | Inception |
| [6] | | MobileNet,VGG, Xception, Inception ResNet v2, Inception |
| [41] | | DarkCovid-Net |
| [42] | | COVID-CAPS |
| [43] | Novel architecture | Lightweight GAN |
| [44] | | DeTraC |
| [45] | | CoroNet |

deep learning networks, deep learning-based classification methods are always considered as "Blackbox" approaches [46]. The state-of-the-art deep learning-based methods have been increasingly used in clinical prediction for healthcare, and have achieved reasonably high performance. However, these models do not provide the explanation to the predictions, leading to a limited understanding of the model prediction [47]. So far, there already have several visual explanation methods for the prediction results from deep learning-based models, such as saliency map [48], classification activation map (CAM) [49], Gradient-CAM(Grad-CAM)[50] and their variants. When using the saliency map for the prediction explanation, it is assumed that the positive gradient of a predicted category with respect to input image should ensure that category. The saliency map could provide a high-resolution gradient result with the same size as the image [51]. Class Activation mapping (CAM) was also a widely used explanation method for the object localisation extraction. In the CAM method, the top fully connected layers in a classification model are replaced with convolutional layers to keep the object locations, thus determining the spatial distribution of discriminative areas for the estimated category. However, the CAM changes the model architecture which requires retraining the model, thus limiting the use of this method. Grad-CAM is a development of the CAM technique that retrains the original architecture and generates weights by pooling the gradient. Since its inception, this technique has been widely applied as it can be used to all deep learning-based classification models [50]. In [23], the author tested Local Interpretable Model-agnostic Explanations (LIME) and CAM methods to explain the prediction from the state-of-the-art deep learning classification methods on CXR datasets. Brunese et al. [24] used the Grad-CAM method to automatically detect the areas of interest in the CXR images corresponding to the COVID-19 disease.

## III. THE PROPOSED METHOD

The aim of this study is two-fold: (1) to classify a CXR image into one of the four classes: Healthy, Bacterial pneumonia, non-COVID Viral pneumonia (ViralN) and COVID-19; and (2) to highlight virus infected areas on the image simultaneously. Therefore, we proposed a novel deep learning framework for classification and pixel-based visual explanation in an end-to-end manner. Fig. 1 provides the overview of the proposed solution consisting of two major components:

1) An Image Preprocessing module including Lung Segmentation and Image Enhancement steps.
   In the lung segmentation step, the lung areas are automatically extracted from CXR images based on a

segmentation model, U-Net. Then, the Contrast Limited Adaptive Histogram Equalization (CLAHE) is applied to the segmented images to enhance their contrast.

2) A CXR-based Deep Neural Network (CXR-Net) for Image Classification and Explanation model.

The proposed deep learning model, CXR-Net, is a convolutional neural network(CNN) based multi-task Encoder-Decoder-Encoder, consisting of two jointly trained encoders for classification. The two encoders are used for the classification task, and the decoder is used to generate visual explanation from the deep features extracted by the encoder. In this study, the first encoder is used to obtain the features of original CXR images while the second encoder is used to extract the features of the reconstructed images from the decoder. The representation image between the two encoders acts as a proxy to visualise the most relevant areas associated with COVID-19 pneumonia diagnosis.

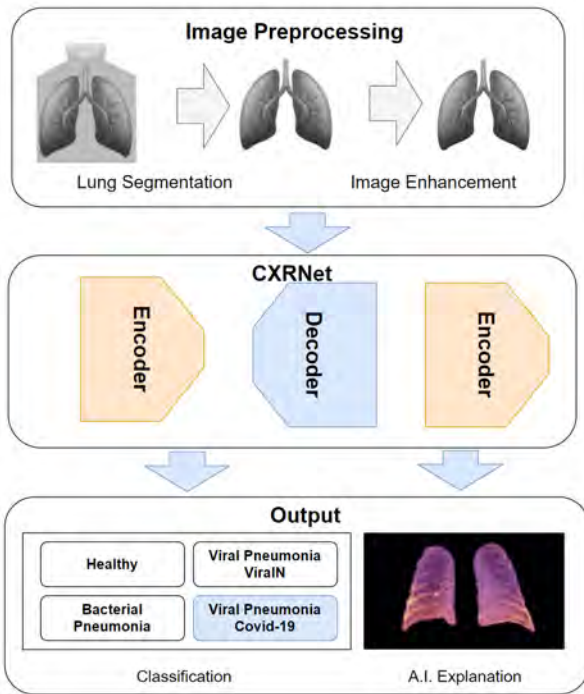These two components are detailed in the following two subsections.



Fig. 1.   The overview of the conceptual framework of the proposed model

## A. Image Preprocessing

*a) Lung Segmentation:* To improve the classification performance, the lung areas are extracted before performing image classification.

In this study, U-Net, a commonly used deep learning-based image segmentation model, was selected. Its structure is shown in Fig. 2, which is the first architecture proposed for biomedical image segmentation [52]. It forms a ladder-like structure by concatenating the encoder feature maps with upsampled feature maps from the decoder at each layer.
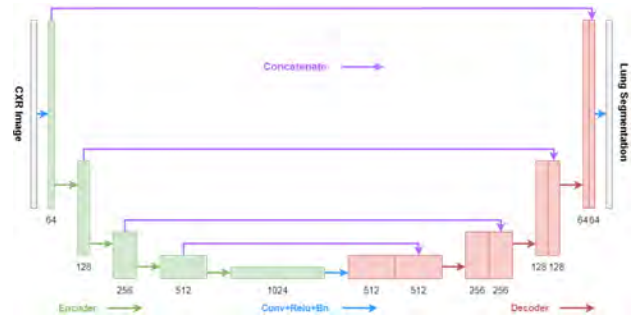


Fig. 2.   The structure of the segmentation model, U-Net

The skip concatenation connections in the design allow the decoder to re-learn relevant characteristics that are lost during the encoder's pooling processes. The U-Net model has a simple and fast design, including a contracting path to capture the environment and a symmetric expanding path to enable accurate localisation. A hybrid loss mixed with Dice and Cross entropy (CE) loss was used as the loss function in the semantic segmentation networks. The loss function in this work is defined as:

$$\text{Loss} = \text{Loss}_{CE} - \log(\text{Loss}_{\text{Dice}}) \tag{1}$$

$$\text{Loss}_{\text{Dice}} = \frac{2 \times TP}{2 \times TP + FP + FN} \tag{2}$$

where TP, FP and FN are true positive, false positive, and false negative, respectively.

*b) Image Enhancement:* The grey X-rays images are typically low contrast, which makes their analyses challenging. Image enhancement is a necessary step for improving the image quality and information content before further processing.

In the process of image enhancement, the most frequent pixel intensity values are often extended to the upper range of the intensity domain [0,255] by conventional histogram equalisation, bringing their cumulative distribution function (CDF) closer to the uniform distribution. However, this method might over-amplify noise in near-constant regions. Instead, in this work, the Contrast Limited Adaptive Histogram Equalization (CLAHE) method was chosen to enhance the contrast of CXR images. Before computing the CDF, it clips the histogram of an image at a predetermined value to spread this portion of the image evenly throughout all histogram bins. Applying the CLAHE to an X-ray image produces visually appealing results, as shown in Fig. 3.
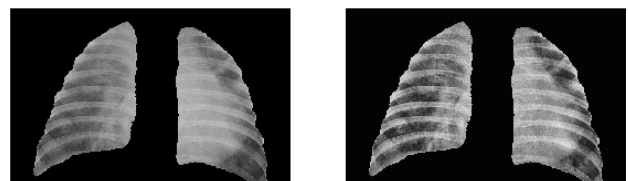


Fig. 3.   Example of CXR images before and after image enhancement with the CLAHE method

### B. A CXR Based Multi-task Deep Neural Network (CXR-Net) for Disease Classification and Explanation

To generate a pixel-level visual explanation result alongside classification, we have proposed a CXR-based deep learning neural Network model for classification and visualisation explanation, named CXR-Net. The high-level conceptual framework of the proposal model is shown in Fig. 4. It is an Encoder-Decoder-Encoder structure, consisting of two encoders and one decoder.

The Encoder-Decoder structure is commonly used in the generator of GAN models [53] and U-Net based segmentation models [52]. Training the encoder-decoder model requires equal-sized labelled samples, which in this work is the annotation of the pathogenic regions. However, accurately labelling the pathogenic areas for COVID-19 is a difficult work because currently the pathogenic area is still not fully understood. We only have category labelling data. Thus, an encoder is added after the encoder-decoder to allow the model to be trained with category samples.

The first encoder in the model is a CNNs structure for feature extraction, which is used to encode the input image into feature representations. Then, the representation is fed into a classifier for identifying the disease types. The decoder is used to reconstruct a heat-map with the same size as the input from the extracted feature representation.

The second encoder has the same structure as the first one, which is used to encode the reconstructed image from the decoder. It is jointly trained with the first encoder to make sure that the reconstructed image represents the most influential areas and features for classification. The second encoder shares the same weights as the first encoder, and uses a fusion loss with a combination of the loss functions of both encoders. During the model training, the parameters of the decoder are iteratively updated to make the generated image keep the most relevant features for identifying the disease.

The model is detailed as follows:

*a) An Encoder-Decoder Structure:* In the model, an encoder-decoder architecture with skip concatenation connections is adopted, as shown in Fig. 4. The network architecture consists of 5 encoder layers and 5 decoder layers. The skip concatenation connections are introduced between each encoder and decoder layers. These connections allow the decoder at each level to re-learn relevant features lost during the encoder's pooling operations. The decoder follows the encoder's structure by adding an up-sampling layer to bring the deep features back to its original size. The objective of upsampling (U) is to generate pixels around and in between existing pixels in order to achieve the required size. The upscale is set to two for each decoder block to ensure that its output has the same size as the forward encoder output. In this model we use an improved method, known as pixel shuffle with ICNR initialisation, which makes the gap filling between pixels much more effectively and avoids generating checkerboard artifacts [54].

The structure of the decoder is shown in Fig. 5 and can be formulated as:

$$\text{Decoder}_n = F\left(U\left(\text{Decoder}_{n-1}\right) + \text{Encoder}_{4-n}\right) \quad (3)$$

where U(Decoder) denotes an up-sampling operation on a decoder's outputs, and F is a combination operation on the concatenation of the feature outputs from the up-sampling operation and the encoder. The F operation contains a rectified linear unit (ReLU) and two convolution blocks. Each convolution block consists of 3x3 2D convolution layers, batch normalization and ReLU. In this study, the leaky ReLU activation function [55] with a negative slope of 0.1 is applied in the decoder to replace the regular ReLU activation. When the unit is not active, it allows for a low gradient. This unit outperforms the traditional ReLU, especially in an encoder-decoder design [56], [57], [58]. The equation of leaky ReLU is defined as :

$$\text{LeakyReLU}(x) = \begin{cases} x \times \text{ slope },x < 0 \\ \qquad x,x \geq 0 \end{cases} \quad (4)$$

*b) Encoders for Classification:* The proposed model has two encoders. The first one directly extracts features from the input image, and the second is to extract the features from the reconstructed image by the decoder. The two encoders share the same weights. After the feature extraction by the two encoders, the extracted feature maps are transformed into a classifier for disease type identification through an average pooling layer and a fully connected layer. The classifier can adopt most of existing CNN classification architectures. In this work, we evaluated four most commonly used encoder architectures, AlexNet [37], VGG16 and 19 [38], ResNet 34 and 50 [32], and Inception-V3 [39]. Their structures are illustrated in Fig. 6.

*c) Fusion Loss:* The loss function of the model is designed to jointly minimise the losses of the two classifiers. The cross-entropy loss is selected as the classification loss function. The fusion loss function is defined as:

$$\text{Loss} = \text{Loss}_{CE1} + \text{Loss}_{CE2} \quad (5)$$

$$\text{Loss}_{CE} = -\sum_i^C t_i \log(p_i) \quad (6)$$

The $Loss_{CE1}$ and $Loss_{CE2}$ are the loss values of the first encoder and the second encoder, respectively, and $p_i$ is the probability of class $i$.

## IV. EXPERIMENTAL EVALUATION

### A. Dataset Description

In this work, 6499 CXR images were used for model training. Among them, there were 636 cases of COVID-19. The dataset was collected from multiple public and private sources: 5,863 cases from [59], 116 COVID-19 cases from [60], [61], 479 COVID cases from [62], [63] and 41 images from COVID-19 patients in the Critical Care unit at the Whiston Hospital, St Helen's & Knowsley NHS Trust, UK. This research has been approved by the Health Research Authority (HRA).

All the images were categorised into one of three classes: Healthy, Bacterial Pneumonia and Viral Pneumonia. The COVID-19 CXR images were labelled as Viral Pneumonia.
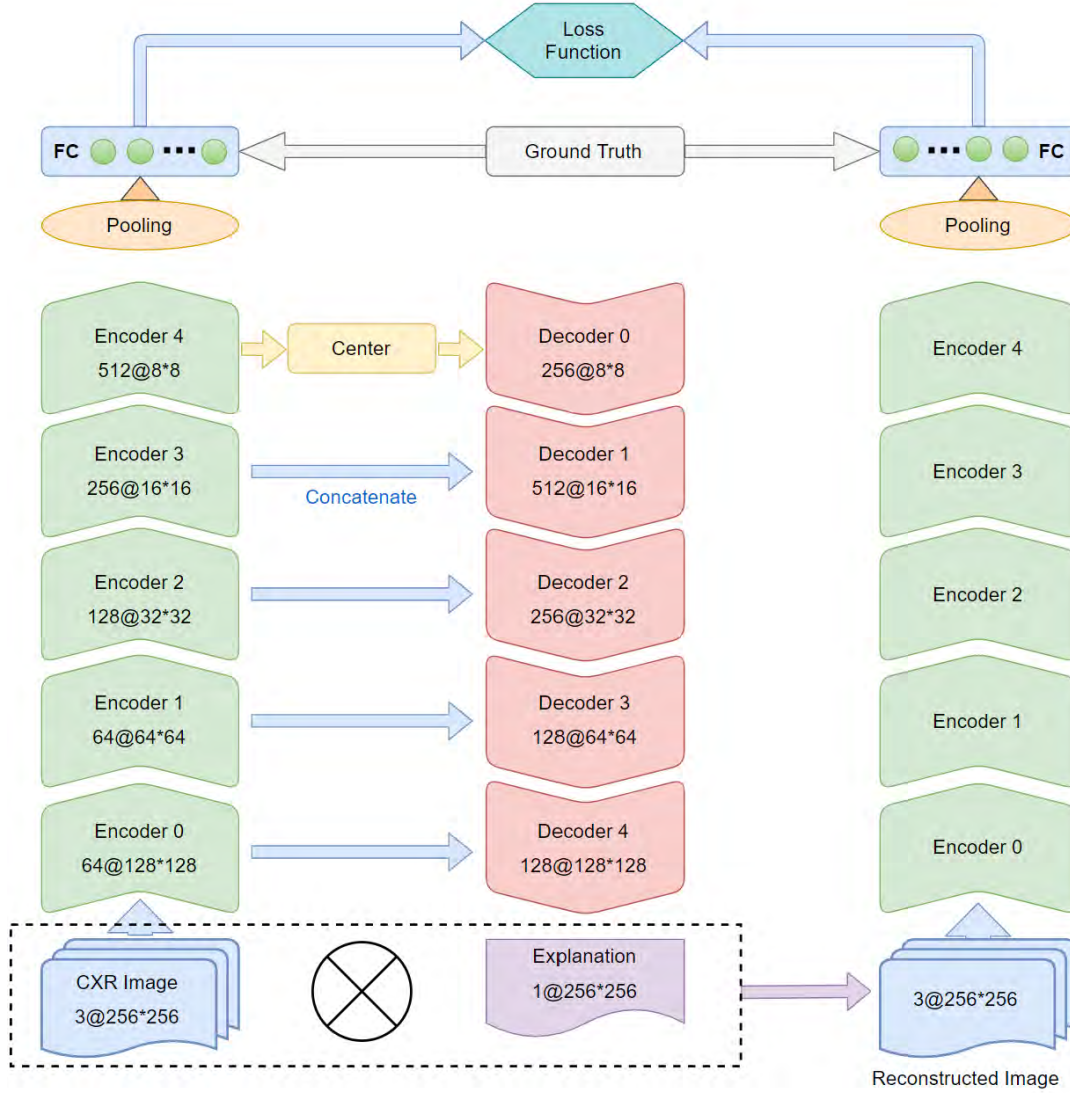
Fig. 4. The architecture of the proposed classification and explanation model, CXR-Net

In this work we split the cases of Viral Pneumonia into two groups, non-COVID-19 viral pneumonia (ViralN) and COVID-19. The images from V7lab provided a pixel-level polygonal lung segmentation on CXR images [64]. Fig. 7 shows some typical samples of CXR images, and Fig. 8 displays two typical examples of lung segmentation labels.

### B. Performance Evaluation Metrics

To evaluate the performance of the lung segmentation model, Intersection over Union (IoU), a commonly used metric, was used. It is defined as:

$$IoU = \frac{\text{Area of Overlap}}{\text{Area of Union}} \tag{7}$$

It is the area of overlap between the predicted segmentation and the ground truth divided by the area of union between the predicted segmentation and the ground truth. IoU ranges in value from 0 to 1.

Due to obvious class imbalance in the dataset (636 COVID19 images vs 5863 Non-COVID19 images), we evaluated the classification performance of the proposed architecture (Especially for COVID-19 recognition) using multiple performance metrics: Sensitivity, Specificity, Positive Predictive Value (PPV), $F1$ score, Average Accuracy and Confusion Matrix. These metrics can be calculated from the true positive (TP), the true negative (TN), the false positive (FP) and the false negative (FN). The metrics are defined as follows:

$$\text{Sensitivity} = \frac{TP}{TP + FN} \tag{8}$$

$$\text{Specificity} = \frac{TN}{TN + FP} \tag{9}$$

$$\text{PPV} = \frac{TP}{TP + FP} \tag{10}$$

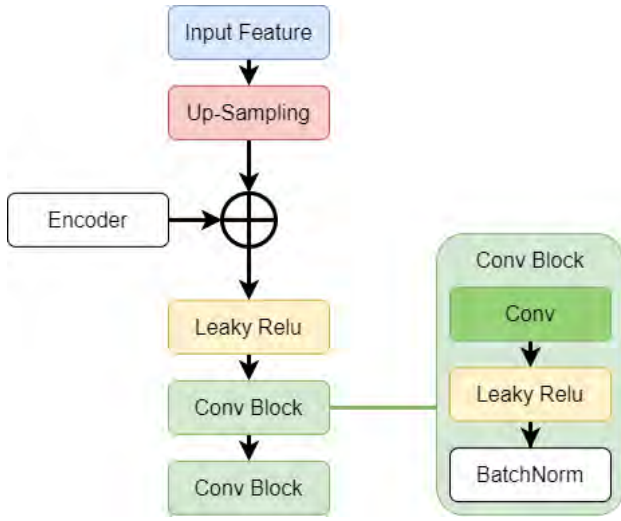$$F1_{\text{score}} = \frac{\text{Sensitivity} \times \text{PPV}}{\text{Sensitivity} + \text{PPV}} \times 2 \tag{11}$$

Fig. 5. The structure of the decoder in the model

$$\text{Accuracy} = \frac{TP+TN}{TP+TN+FP+FN} \tag{12}$$

We also used the receiver operating characteristics (ROC) and the area under the curve (AUC) for performance evaluation of classification models. ROC plots are generated using false positive rates and true positive rates, after plotting the region of points under the curve, called AUC. If the AUC value is close to 1, the model will be considered to be performing well; if the AUC value is close to 0, then the model will be considered to perform poorly. In this paper, both ROC and AUC for evaluating COVID-19 detection performance are provided.

Furthermore, Probability Perturbation Curve (PPC) was calculated to evaluate the quality of visual explanation. The essence of the PPC is to proportionally remove the important regions in an image to produce the perturbations of variables to the original image, and then to evaluate how the classification performance responds to the changes of different portions in pixel removals (perturbations). For instance, when removing the large portion of an important region from an image, the classification performance is supposed to be lower than that without removal. Therefore, the greater the perturbation to the classifier, the more important that removed region. Here, the value of a pixel in the visualisation result determines its importance for classification. Starting from removing those pixels with high values in the explanation result, a perturbed images will be generated. Then, the perturbed image is fed to the trained classifier to get the probability of its corresponding type. A curve can be plotted following the change of points with coordinates (x, p(f(x))) during the pixel removal procedure. The coordinate, x, starts from 1 to 0, and the coordinate, f(x), denotes the removal procedure in which all the pixels with a value of x are replaced with zeros. So, f(0) means no change to the original image, and f(1) means all the pixels with a value of 1 (the most important regions detected by models) will be assigned with zeros. $p(f(x))$ is the probability calculated from the classifier based on the processed image.

This approach will be used for all COVID-19 images, and the probabilities are averaged to produce the curve. The area over probability perturbation curve (AOPPC) is calculated to evaluate the quality of visual explanation and is formulated as:

$$AOPPC = \frac{1}{10}\sum_{i=1}^{10}\sum_{x=0.1}^{1}\left(p(f(0))-p(f(x))\right) \tag{13}$$

### C. Model Training Setup

This model was developed using Pytorch 1.6 and Fastai [65]. All the experiments were trained on a workstation equipped with an Intel®Xeon®E Processor E5-2650, NVIDIA GeForce RTX 2080 Ti, and 64GB of RAM. Fastai is a deep learning model training library that can quickly and easily provide standardised training results in deep learning domains. It provides researchers with custom APIs that can be mixed and matched to build new models. In this work, the optimisation technique used in the model was Adam (A Method for Stochastic Optimisation) with a batch size of 12. In general, the learning rate (LR) controls how much the weights of the network are adjusted with respect to the loss gradient. A bigger LR will allow for faster model training with large steps, but may fail to find the best model. A small LR will lead to a long training time. Since we utilised transfer learning to accelerate model training in this work, a learning rate finder [66] was used to search the best model learning rate. Fig. 9 shows the relationship between the loss and LR. From the observation, it can be found that the best LR is $1\times10^{-3}$. Thus, we initially set a starting learning rate of $1\times10^{-3}$ for model training. Then, the learning rate was gradually decreased to $1\times10^{-6}$ during the iteration.

For each model, we trained 100 epochs and saved the weights for the model generating best validation results. To validate our method, we applied a 5-fold cross-validation. The model was trained and tested five times, and the database was split in a ratio of 80 : 20. As a result, we obtained the mean and its standard deviation. This allowed a more appropriate model analysis and made it possible to avoid overfitting problems, as the entire database was trained at least once during the 5-fold validation procedure. The Pseudo-Algorithm of the model training is shown in Fig. 10.

### D. Experiment Evaluation

In this study, four experiments were conducted to evaluate the model performance from four different aspects: a) model classification performance, b) the effect of lung segmentation on classification performance, c) model compatibility and efficiency, and d) model explainability.

*a) Model Classification Performance:* In this test, the model was trained on CXR images without pre-segmentation. Six most commonly used CNN architectures and a standard U-Net encoder part were considered for the encoder. They included AlexNet, VGG-16, VGG-19, ResNet-34, ResNet-50 and Inception-V3. The standard U-Net structure can be considered as a simplified VGG-16 with two convolutions in
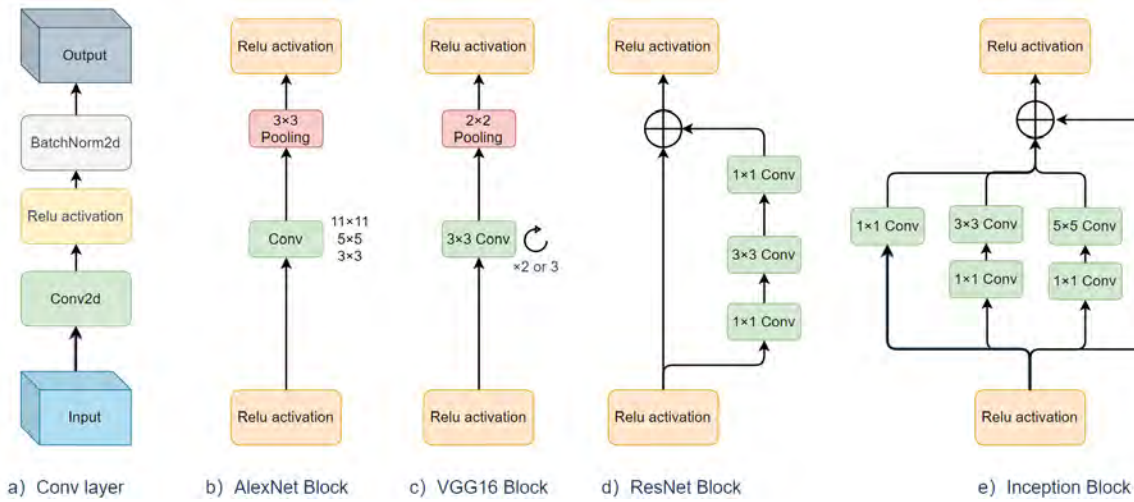
Fig. 6. The schematic diagrams of AlexNet, VGG16, ResNet and Inception encoder blocks
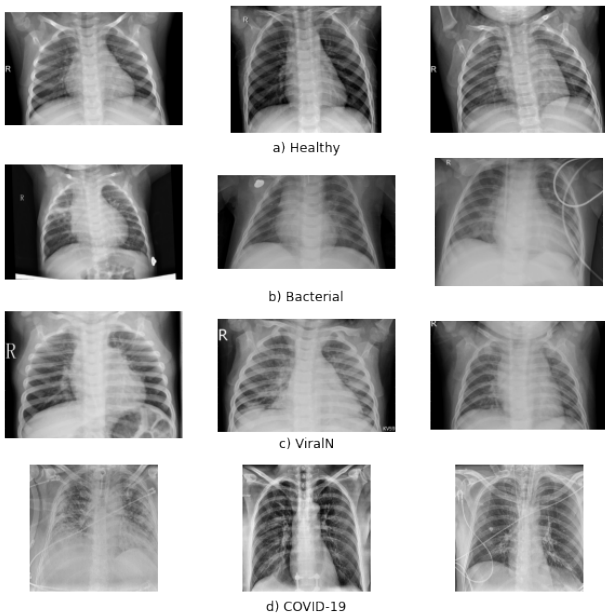


Fig. 7. CXR image samples of a) Healthy, b) Bacterial, c) Viral and d) COVID-19 cases in the datasets.
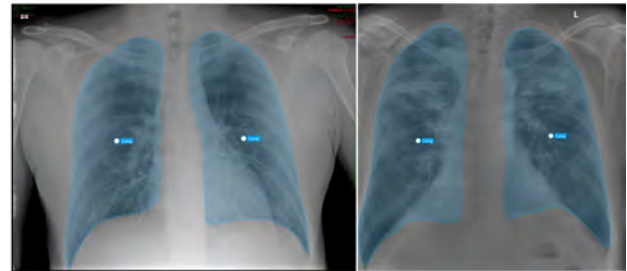


Fig. 8. Two examples of pixel-level lung segmentation on the CXR images. The left one is the segmented result of a CXR image from a non-COVID-19 patient, and the right one is the segmented result of a CXR image from a COVID-19 patient. The lung segmentation results are superimposed on the raw CXR images.



Fig. 9. The relationship between the loss rate and the learning rate

each layer. Table. III shows a comparison of average accuracy (ACC) and model parameters (Giga Multiply-accumulate operation (Gmac) and the number of parameters) when different CNN architectures are chosen for the encoder. Among them, the models with ResNet-50 or Inception-V3 architectures in the encoder achieve the highest average accuracy. A better performance of the model with ResNet-50 (50 layers) over the model with ResNet-34 (34 layers) shows that a deeper architecture may boost the performance. Due to the limitation of GPU memory, we did not choose a more complex architecture than ResNet-50.

AUC and ROC were also used for evaluating the performance of COVID diagnosis. Fig. 11 shows the ROCs of the models when six different CNN architectures are chosen for the encoder. With an AUC of 0.96, the models using ResNet-50 or Inception-V3 in the encoder show a better classification performance.
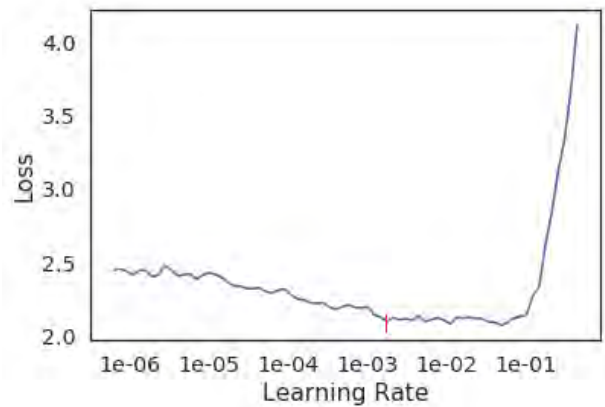
*b) The Effect of Lung Segmentation on Model Performance:* The lung areas in CXR images are the regions of interest (ROI) for the COVID-19 diagnosis. It is expected that the model classification performance can be improved by only focusing on lung areas. To verify this hypothesis, we compared the classification results of the proposed model

**Algorithm 1** Pseudo-Algorithm of CXRNet

**Input:**
    $x\_batch$: One batch CXR images;
    $y\_batch$: One batch Diagnostic results;
    $LungSeg$: Lung Segmentation model;
    $CLAHE$: Contrast Limited Adaptive Histogram Equalization;
    $CXRNet$: CXRNet COVID-19 diagnosis Network;

**Output:**
    $t\_batch$: One batch predict results;
    $z\_batch$: One batch activation maps;

1: set $LearningRate = 0.001$; # Learning Rate gradually decreased to $1 \times 10^{-6}$ during the iteration;
2: set $BS = 12$ # Batch size=12;
3: set $Optimizer = Adam$;
4: set $Epochs = 100$;
5: **for** epoch in Epochs **do**
6:     **for** x, y in $x\_batch$, $y\_batch$ **do** # One batch training
7:         $x1 = LungSeg(x)$ # Lung Segmentation
8:         $x1 = CLAHE(x1)$ # Image Enhancement
9:         $x1 = Aug(x1)$ # Normal augmentation
10:        $t1, t2, z = CXRNet(x1)$ # result of CXRNet
11:        $loss = L(t1, y) + L(t2, y)$ # Cross-entropy Loss function
12:        loss.backward() # Back-propagate
13:        Update(CXRNet.params)
14:     **end for**
15: **end for**

Fig. 10.   The Pseudo-Algorithm of the model training

TABLE III
CLASSIFICATION ACCURACY AND MODEL PARAMETER COMPARISON OF MODELS WITH DIFFERENT CNN ARCHITECTURES FOR THE ENCODER

| ModelName | Gmac | Params(M) | Acc$\pm$ Std |
|-----------|------|-----------|--------------|
| AlexNet | 0.72 | 61.1 | 0.785$\pm$ 0.046 |
| U-Net | 11.36 | 133.06 | 0.785$\pm$ 0.042 |
| VGG-16 | 15.53 | 138.37 | 0.796$\pm$ 0.102 |
| VGG-19 | 19.7 | 143.68 | 0.815$\pm$ 0.088 |
| ResNet-34 | 3.68 | 21.8 | 0.831$\pm$ 0.147 |
| ResNet-50 | 4.12 | 25.56 | 0.879$\pm$ 0.012 |
| Inception-V3 | 2.85 | 27.16 | 0.878$\pm$ 0.019 |

through training it on CXR datasets with or without lung segmentation, respectively.

A U-Net semantic segmentation model was trained on the same CXR dataset to extract lung areas. In this study, the IoU accuracy reached 0.925, close to the results from other works [13], [14], [28].

Fig. 12 a) shows a comparison of classification accuracy when two different depth ResNet models (34 and 50 layers) are trained on original images and lung segmented images, respectively. The results show that the classification performance of the model has been improved by training on lung segmented images instead of original images. In addition, increasing the model depth can improve the classification performance. Fig. 12 b) shows the training loss curves of ResNet50 based encoder models trained on original and segmented images, respectively. It can be found that the loss is lower when the model is trained on the segmented images rather than their original images. This confirms that the model performs better on the segmented images in the lung disease detection.

The effect of pre-segmentation on the model performance can be further evaluated with their confusion matrix, as shown in Fig. 13. In a confusion matrix, each value represents the number of predictions produced by the model in which it properly or incorrectly identifies the classes; each column shows the predicted results of the model for one class. The
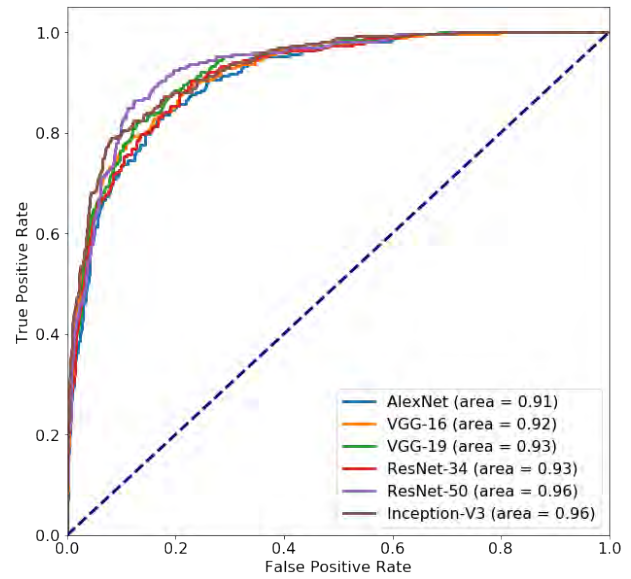


Fig. 11.   The ROC curves in the COVID-19 detection for the models with six different CNN architectures in the encoder

Sensitivity, Specificity, PPV and F1 score are provided in Table IV for the ResNet50-based encoder trained on original and segmented CXR images, respectively. From the Confusion Matrix, we can find that the model performs well in the detection of COVID-19. 128 out of 130 and 129 out of 130 cases are correctly identified by the model trained on original and lung segmented CXR images, respectively. When the model is trained on the segmented images, it achieves an average accuracy of 0.879 for all classes and an F1-score of 0.989 for COVID-19. However, bacterial and normal Viral pneumonia are harder to be distinguished by the model. 61 out of 537 bacterial pneumonia CXR images are incorrectly identified as non-COVID-19 viral pneumonia, while 54 out of 267 non-COVID-19 pneumonia are incorrectly identified as bacterial pneumonia.
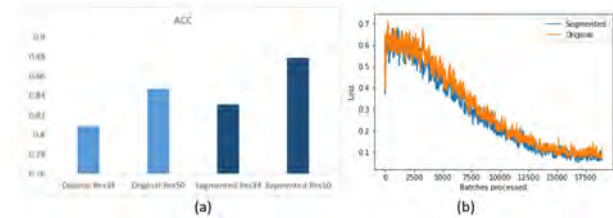


Fig. 12.   A comparison of model performance of two ResNet models trained on original images and lung segmented images, respectively : a) classification accuracy and b) the training loss trend

*c) Model Compatibility and Efficiency:* One of the key challenges for deep learning-based methods is the compatibility of models from their development environments to practical clinical applications. To investigate the compatibility and efficiency of the proposed models, we deployed the model to three different environments: AWS Cloud Computing Services, Local CPU and GPU machines. We compared the running time of the proposed model on these three different computing platforms. As shown in Table V, the runtime of the

TABLE IV
CLASSIFICATION RESULTS FOR LUNG DISEASES FROM THE MODELS TRAINED ON ORIGINAL IMAGES AND SEGMENTED IMAGES

| | Original Dataset | | | | Segmented Dataset | | | |
|---|---|---|---|---|---|---|---|---|
| | Sensitivity | Specificity | PPV | F1-score | Sensitivity | Specificity | PPV | F1-score |
| Healthy | 0.974±0.059 | 0.957±0.083 | 0.881±0.06 | 0.925±0.056 | 0.967±0.046 | 0.974±0.049 | 0.925±0.036 | 0.946±0.036 |
| Bacterial | 0.838±0.079 | 0.905±0.092 | 0.87±0.075 | 0.854±0.034 | 0.868±0.102 | 0.919±0.103 | 0.891±0.102 | 0.879±0.076 |
| ViralN | 0.655±0.071 | 0.918±0.093 | 0.686±0.071 | 0.67±0.053 | 0.745±0.088 | 0.931±0.119 | 0.748±0.052 | 0.747±0.023 |
| Covid | 0.985±0.047 | 0.998±0.054 | 0.985±0.055 | 0.985±0.033 | 0.992±0.147 | 0.998±0.141 | 0.985±0.148 | 0.989±0.089 |
| Accuracy | 0.847±0.023 | | | | 0.879±0.019 | | | |



Fig. 13.    Confusion matrix from the ResNet50-based model trained on Original and Lung Segmented CXR images, respectively

model on these three platforms is in the range of 5 seconds to 1 minutes. This demonstrates that the deployment of our deep learning model to promote the detection of COVID-19 pneumonia from CXR images is achievable using regular computers and cloud services, and therefore it is considered scalable even in underdeveloped and remote hospitals.

TABLE V
A COMPARISON OF RUNTIME OF THE PROPOSED MODEL ON THREE DIFFERENT COMPUTATIONAL ENVIRONMENTS

| Machine | Specifications | Run time |
|---|---|---|
| AWS (CPU) | 2 virtual central processing units (vCPUs) and 8GB memory | 60 sec ± 10 sec |
| Local Server (CPU) | 2.3GHz Intel Core i7 and 16GB memory | 45 sec ± 5 sec |
| Local Server (GPU) | NVIDIA GeForce RTX 2080 Ti | 5 sec ± 1 sec |

*d) Model Explainability:* The heatmap of classification activation and the AOPPC were used to evaluate the performance of our proposed model for visual explanation and classification. It was also compared with two most commonly used DCNN explanation methods: Saliency map and Grad-CAM.
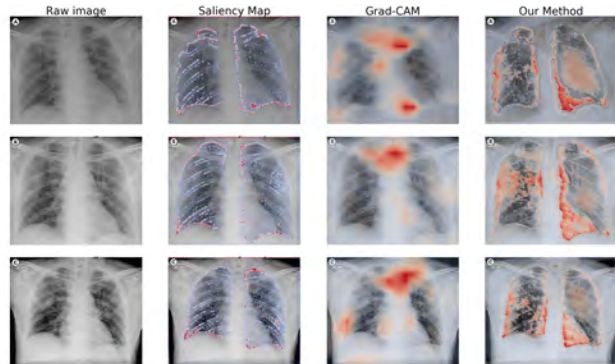


Fig. 14.    Three typical examples of class activation heatmaps from three visualisation algorithms (a) Saliency Map (b) Grad-CAM (c) Our method

Fig. 14 presents three typical examples of class activation heatmaps from existing methods (Saliency map and Grad-CAM) and our proposed approach. Compared to the Saliency map and Grad-CAM approaches, our proposed algorithm provides shaper heatmaps due to its capability to generate pixel-level results. The saliency map results are more noisy because it uses gradients to measure the sensitivities of pixels rather than their contributions to classification. Although the Grad-CAM can globally localise important regions, it has missed some areas identified by the proposed method. The missed identification may be due to the low-resolution features used by the Grad-CAM method when propagating the contributions of class activation from the last convolution layer in the models.
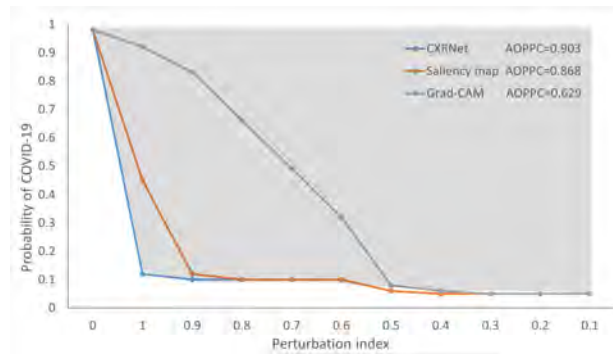


Fig. 15.    The probability perturbation curves (PPC) and the area over probability perturbation curve (AOPPC) of three visual explanation methods. The perturbation index in x axis shows the level of perturbation on images by removing the regions with a pixel value of x. The y axis presents the probability of COVID-19 predicted by the trained classifier on the perturbed images.

Fig. 15 shows the PPCs from three visualization approaches. The AOPPCs from the Salient Map, Grad-Cam and our methods are 0.629, 0.868 and 0.903, respectively. Our method has the highest score in evaluating the quality of visual explanation for the COVID-19 detection.

## V. DISCUSSION

In this work, we have proposed a pixel level explainable classification model (CXR-Net) for COVID-19 pneumonia diagnosis. This is a two-task model. The first task is to predict classification results of CXR images for the diagnosis of lung diseases. The second one is to generate an explainable mask to highlight the areas related to classification decision making. In this section, we will discuss the performance of the model on these two tasks, classification and visual explanation.

TABLE VI
COMPARATIVE PERFORMANCE OF THE PROPOSED METHOD AND SEVEN COMPETITORS

| References | Modality | Subject | Method | Covid performance | |
| --- | --- | --- | --- | --- | --- |
| | | | | Sensitivity | Specificity |
| [67] | Classification | 1323 COVID, 7512 All | CNN | 93.98% | 99.65% |
| [68] | Classification | 576 COVID, 6423 All | CNN+Aquila Optimizer Algorithm | 86.60% | 89.40% |
| [69] | Classification | 184 COVID, 5128 All | CNN | 94.00% | 99.30% |
| [7] | Classification | 430 COVID, 1130 All | CNN+Transfer learning | - | 96.00% |
| [70] | Classification+explanation | 184 COVID, 5000 All | CNN+ Saliency map | 92.90% | 98.00% |
| [71] | Classification+explanation | 219 COVID, 5520 All | CNN+Grad-Cam | 92.50% | 98.66% |
| [6] | Classification+explanation | 459 COVID, 5877 All | CNN+Grad-Cam | 87.80% | 98.00% |
| Our method | Classification+explanation | 636 COVID, 6499 All | CNN+Encoder-Decoder | 98.60% | 99.20% |

## A. Performance of CXR-Net for COVID Diagnosis

Our model, CXR-Net, consists of two main steps for COVID-19 diagnosis: Lung segmentation and lung disease classification. The Lung segmentation is part of the image pre-processing. We selected the most commonly used semantic segmentation model, U-Net, for lung segmentation on CXR images. The segmented images were then fed into the encoder for lung disease classification. Our results demonstrated that using segmented images can significantly improve the diagnostic accuracy of the model. The diagnostic accuracy was improved by 2.2% and 3.2% on ResNet-34 and 50 models, respectively. Similar results have also been demonstrated in previous studies [72], [73]. However, fine-grained lung segmentation still remains a challenging task. Especially in patients with severe lung diseases, the segmentation accuracy could be poor. Fig. 16 shows two examples of erroneous lung segmentation results on CXR images of COVID-19 patients where a part of lung areas is not properly segmented. This could adversely affect the accuracy of diagnosis. We will continue to explore more effective and accurate lung segmentation algorithms in future work.
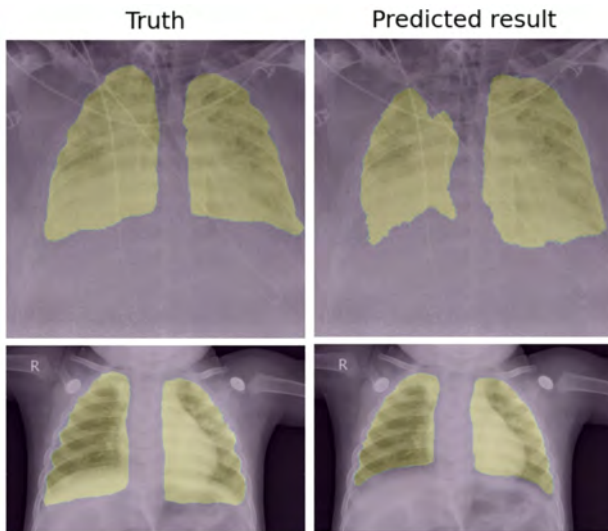


Fig. 16. Two examples of wrong segmentation results of lungs

In this study, CXR-Net is designed to allow a flexible choice for the encoder's network structure. To evaluate the effect of different network structures on classification accuracy, we selected four commonly used CNN structures, including AlexNet , VGG , ResNet and Inception, The computational complexity and the number of parameters in each encoder

are shown in Table III. AlexNet and VGG use plain and linear CNN structures with large kernel sizes (5 and 7). The results show that a large kernel size dramatically increases the computational complexity and the number of parameters. However, this does not result in a significantly improvement on the classification accuracy of the model.

Compared to the plain structure design in AlexNet and VGG, the residual connection introduced in ResNet allows the gradient to flow through the structure to solve the problem of vanishing gradient in deep neural networks which may cause the failure of model training or convergence [32]. As shown in Table III, this structure significantly improves the model depth and its accuracy. Compared with ResNet models, the Inception model increases the network width, but does not improve the classification accuracy in this study.

## B. Model Explainability

COVID-19 pneumonia can increase the X-ray opacity of lungs, which shows as white on Chest radiography. Therefore, multi-focal ground-glass opacity, linear opacities, and consolidation can be seen as evidence for the existence of COVID-19 infection [74]. Accurately identifying these areas on CXR images will bring more robust and confident diagnosis for patients.

The second task of the CXR-Net is to generate an explainable mask for more trustful COVID-19 diagnosis. Compared with two most commonly used interpretable methods, Saliency map and Grad-CAM, our model can generate more detailed, high-resolution masks of the pathogenic regions and has achieve the highest score in terms of the AOPPC value in quantifying the performance of visual explanation.

Fig. 17 shows two examples of our heatmap results along with manual annotations on CXR images of COVID-19 pneumonia patients. On the left column, the red polygons on the raw images mark the glass opacities, the bilateral dense peripheral consolidation and the linear opacity area annotated by two radiologists. The middle and right columns show the heatmaps by Grad-CAM and our method. As shown in Fig. 17, due to the low resolution of the Grad-CAM, it is difficult to clearly visualise the disease-related areas. However, all the ground-glass opacity and linear opacity areas annotated by the radiologists are highlighted by our model.

## C. Model Comparison

It is unfair to perform a direct comparison between different methods due to the use of different datasets and experiment
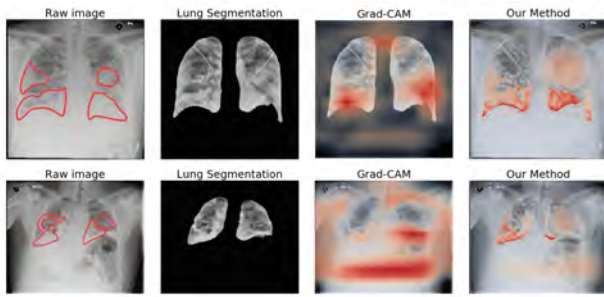
Fig. 17. The CXR images of a patient with COVID-19 pneumonia. On the left column, the red polygons on the images mark the ground glass opacities, the bilateral dense peripheral consolidation and the linear opacity areas, annotated by radiologists. The right column presents the heatmap from our method. The heatmaps from the Grad-CAM model are added on the third column for comparison.

environments. Therefore, we have only indirectly compared our model with seven recent machine learning-based COVID-19 diagnosis methods [6], [7], [67], [68], [69], [69], [70], [71]. The results are shown in Table VI. It can be found that all the listed deep learning-based models achieve satisfactory accuracy in the diagnosis of COVID-19. However, our model outperforms other existing approaches in terms of both sensitivity and specificity. Additionally, our datasets are acquired from both publicly available data and private hospital data, which contains more COVID-19 cases, compared to the datasets used in the existing methods except for [67].

## VI. CONCLUSION AND FUTURE SCOPE

In this work, we have proposed a pixel level explainable classification model (CXR-Net) for COVID-19 pneumonia diagnosis which are validated using real clinical data. It is based on an encoder-decoder-encoder architecture, enabling a multitask learning for accurate and explainable disease classification. The experimental results have demonstrated that the proposed method can achieve a reasonably high accuracy on classification using lung segmented CXR images. The model achieved an average accuracy of 0.879, and the Sensitivity, Specificity, PPV and F1-score of COVID-19 are 0.992, 0.998, 0.985 and 0.989, respectively. Moreover, the model can generate sharper and more precise visualisation images, compared to another two most popular visual explanation approaches, Salient Map and Grad-Cam. The model-generated high-resolution heat maps to highlight the suspected abnormal regions match clinical annotations, which could help explain the classifier's decision and diagnosis of COVID-19 pneumonia from the model. A clinically acceptable computing time provided by the model in three different operational environments demonstrates its suitability for clinical applications, even in underdeveloped and remote areas. Overall, the proposed model has a great potential to assist radiologists in screening patients with suspected COVID-19 within a reasonable time scale, thereby reducing the waiting time for clinical decisions. Currently, the CXR image data on COVID is still limited, compared to other pneumonia data. In the future, we will collect more COVID-19 related CXR data for model

training in order to increase the generalisability of the model and make them publicly accessible to the community.

## ETHICAL STATEMENTS

## ACKNOWLEDGMENT

## REFERENCES

[1] W. Taylor, Q. H. Abbasi, K. Dashtipour, S. Ansari, A. Shah, A. Khan, and M. A. Imran, "A review on the state of the art in non contact sensing for covid-19," *arXiv:2007.16063 [physics]*, 7 2020, arXiv: 2007.16063. [Online]. Available: http://arxiv.org/abs/2007.16063

[2] A. Tahamtan and A. Ardebili, "Real-time rt-pcr in covid-19 detection: issues affecting the results," *Expert review of molecular diagnostics*, vol. 20, no. 5, pp. 453–454, 2020.

[3] M. Teymouri, S. Mollazadeh, H. Mortazavi, Z. N. Ghale-Noie, V. Keyvani, F. Aghababaei, M. R. Hamblin, G. Abbaszadeh-Goudarzi, H. Pourghadamyari, S. M. R. Hashemian *et al.*, "Recent advances and challenges of rt-pcr tests for the diagnosis of covid-19," *Pathology-Research and Practice*, vol. 221, p. 153443, 2021.

[4] S. Kadry, V. Rajinikanth, S. Rho, N. S. M. Raja, V. S. Rao, and K. P. Thanaraj, "Development of a machine-learning system to classify lung ct scan images into normal/covid-19 class," *arXiv:2004.13122 [cs, eess, stat]*, 4 2020, arXiv: 2004.13122. [Online]. Available: http://arxiv.org/abs/2004.13122

[5] P. K. Sethy and S. K. Behera, "Detection of coronavirus disease (covid-19) based on deep features," *Preprints*, vol. 2020030300, p. 2020, 2020.

[6] L. R. Baltazar, M. G. Manzanillo, J. Gaudillo, E. D. Viray, M. Domingo, B. Tiangco, and J. Albia, "Artificial intelligence on covid-19 pneumonia detection using chest xray images," *Plos one*, vol. 16, no. 10, p. e0257884, 2021.

[7] M. Berrimi, S. Hamdi, R. Y. Cherif, A. Moussaoui, M. Oussalah, and M. Chabane, "Covid-19 detection from xray and ct scans using transfer learning," in *2021 International Conference of Women in Data Science at Taif University (WiDSTaif)*. IEEE, 2021, pp. 1–6.

[8] M. L. Holshue, C. DeBolt, S. Lindquist, K. H. Lofy, J. Wiesman, H. Bruce, C. Spitters, K. Ericson, S. Wilkerson, and A. Tural, "First case of 2019 novel coronavirus in the united states," *New England Journal of Medicine*, 2020, publisher: Mass Medical Soc.

[9] L. Orioli, M. P. Hermans, J.-P. Thissen, D. Maiter, B. Vandeleene, and J.-C. Yombi, "Covid-19 in diabetic patients: Related risks and specifics of management," *Annales d'Endocrinologie*, vol. 81, no. 2, pp. 101–109, 6 2020.

[10] S. Basu, S. Mitra, and N. Saha, "Deep learning for screening covid-19 using chest x-ray images," *medRxiv*, p. 2020.05.04.20090423, 5 2020, publisher: Cold Spring Harbor Laboratory Press.

[11] Y. Feng, H. S. Teh, and Y. Cai, "Deep learning for chest radiology: A review," *Current Radiology Reports*, vol. 7, no. 8, 2019, [Online; accessed 2020-09-12]. [Online]. Available: https://link.springer.com/epdf/10.1007/s40134-019-0333-9

[12] D.-P. Fan, T. Zhou, G.-P. Ji, Y. Zhou, G. Chen, H. Fu, J. Shen, and L. Shao, "Inf-net: Automatic covid-19 lung infection segmentation from ct images," *arXiv:2004.14133 [cs, eess]*, 5 2020, arXiv: 2004.14133. [Online]. Available: http://arxiv.org/abs/2004.14133

[13] G. Gal, B. Maga, and A. Lukcs, "Attention u-net based adversarial architectures for chest x-ray lung segmentation," *arXiv:2003.10304 [cs, eess]*, 3 2020, arXiv: 2003.10304. [Online]. Available: http://arxiv.org/abs/2003.10304

[14] N. Saeedizadeh, S. Minaee, R. Kafieh, S. Yazdani, and M. Sonka, "Covid tv-unet: Segmenting covid-19 chest ct images using connectivity imposed u-net," *arXiv:2007.12303 [cs, eess]*, 7 2020, arXiv: 2007.12303. [Online]. Available: http://arxiv.org/abs/2007.12303

[15] R. Selvan, E. B. Dam, N. S. Detlefsen, S. Rischel, K. Sheng, M. Nielsen, and A. Pai, "Lung segmentation from chest x-rays using variational data imputation," *arXiv:2005.10052 [cs, eess, stat]*, 7 2020, arXiv: 2005.10052. [Online]. Available: http://arxiv.org/abs/2005.10052

[16] B. Cheng, M. D. Collins, Y. Zhu, T. Liu, T. S. Huang, H. Adam, and L.-C. Chen, "Panoptic-deeplab: A simple, strong, and fast baseline for bottom-up panoptic segmentation," *arXiv:1911.10194 [cs]*, 3 2020, arXiv: 1911.10194. [Online]. Available: http://arxiv.org/abs/1911.10194

[17] M. K. Hasan, M. A. Alam, M. T. E. Elahi, S. Roy, and S. R. Wahid, "Cvr-net: A deep convolutional neural network for coronavirus recognition from chest radiography images," *arXiv:2007.11993 [cs, eess]*, 7 2020, arXiv: 2007.11993. [Online]. Available: http://arxiv.org/abs/2007.11993

[18] A. Shelke, M. Inamdar, V. Shah, A. Tiwari, A. Hussain, T. Chafekar, and N. Mehendale, "Chest x-ray classification using deep learning for automated covid-19 screening," Tech. Rep., 6 2020, dOI: 10.1101/2020.06.21.20136598. [Online]. Available: http://medrxiv.org/lookup/doi/10.1101/2020.06.21.20136598

[19] L. Wang, Z. Q. Lin, and A. Wong, "Covid-net: A tailored deep convolutional neural network design for detection of covid-19 cases from chest x-ray images," *Scientific Reports*, vol. 10, no. 1, pp. 1–12, 2020.

[20] P. Rajpurkar, J. Irvin, R. L. Ball, K. Zhu, B. Yang, H. Mehta, T. Duan, D. Ding, A. Bagul, C. P. Langlotz, B. N. Patel, K. W. Yeom, K. Shpanskaya, F. G. Blankenberg, J. Seekins, T. J. Amrhein, D. A. Mong, S. S. Halabi, E. J. Zucker, A. Y. Ng, and M. P. Lungren, "Deep learning for chest radiograph diagnosis: A retrospective comparison of the chexnext algorithm to practicing radiologists," *PLOS Medicine*, vol. 15, no. 11, p. e1002686, 11 2018, publisher: Public Library of Science.

[21] D. A. D. Júnior, L. B. da Cruz, J. O. B. Diniz, G. L. F. da Silva, G. B. Junior, A. C. Silva, A. C. de Paiva, R. A. Nunes, and M. Gattass, "Automatic method for classifying covid-19 patients based on chest x-ray images, using deep features and pso-optimized xgboost," *Expert Systems with Applications*, vol. 183, p. 115452, 2021.

[22] T. Chen, T. He, M. Benesty, V. Khotilovich, Y. Tang, H. Cho, K. Chen *et al.*, "Xgboost: extreme gradient boosting," *R package version 0.4-2*, vol. 1, no. 4, pp. 1–4, 2015.

[23] M. M. Ahsan, K. D. Gupta, M. M. Islam, S. Sen, M. L. Rahman, and M. S. Hossain, "Study of different deep learning approach with explainable ai for screening patients with covid-19 symptoms: Using ct scan and chest x-ray image dataset," *arXiv:2007.12525 [cs, eess]*, 7 2020, arXiv: 2007.12525. [Online]. Available: http://arxiv.org/abs/2007.12525

[24] L. Brunese, F. Mercaldo, A. Reginelli, and A. Santone, "Explainable deep learning for pulmonary disease and coronavirus covid-19 detection from x-rays," *Computer Methods and Programs in Biomedicine*, vol. 196, p. 105608, 11 2020.

[25] B. Ghoshal and A. Tucker, "Estimating uncertainty and interpretability in deep learning for coronavirus (covid-19) detection," *arXiv:2003.10769 [cs, eess, stat]*, 3 2020, arXiv: 2003.10769. [Online]. Available: http://arxiv.org/abs/2003.10769

[26] J. Zhang, Y. Xie, Z. Liao, G. Pang, J. Verjans, W. Li, Z. Sun, J. He, Y. Li, C. Shen, and Y. Xia, "Viral pneumonia screening on chest x-ray images using confidence-aware anomaly detection," *arXiv:2003.12338 [cs, eess]*, 6 2020, arXiv: 2003.12338. [Online]. Available: http://arxiv.org/abs/2003.12338

[27] P. M. Gordaliza, A. Muoz-Barrutia, M. Abella, M. Desco, S. Sharpe, and J. J. Vaquero, "Unsupervised ct lung image segmentation of a mycobacterium tuberculosis infection model," *Scientific Reports*, vol. 8, no. 1, p. 9802, 6 2018, number: 1 publisher: Nature Publishing Group.

[28] A. Sarkar, J. Vandenhirtz, J. Nagy, D. Bacsa, and M. Riley, "Detection of covid-19 from chest x-rays using deep learning: Comparing cognex visionpro deep learning 1.0 software with open source convolutional neural networks," *arXiv:2008.00597 [eess]*, 8 2020, arXiv: 2008.00597. [Online]. Available: http://arxiv.org/abs/2008.00597

[29] G. Huang, Z. Liu, L. van der Maaten, and K. Q. Weinberger, "Densely connected convolutional networks," *arXiv:1608.06993 [cs]*, 1 2018, arXiv: 1608.06993. [Online]. Available: http://arxiv.org/abs/1608.06993

[30] X. Wang, Y. Peng, L. Lu, Z. Lu, M. Bagheri, and R. M. Summers, "Chestx-ray8: Hospital-scale chest x-ray database and benchmarks on weakly-supervised classification and localization of common thorax diseases," *2017 IEEE Conference on Computer Vision and Pattern Recognition (CVPR)*, pp. 3462–3471, 7 2017, arXiv: 1705.02315.

[31] I. M. Baltruschat, H. Nickisch, M. Grass, T. Knopp, and A. Saalbach, "Comparison of deep learning approaches for multi-label chest x-ray classification," *Scientific Reports*, vol. 9, no. 1, p. 6381, 4 2019, number: 1 publisher: Nature Publishing Group.

[32] K. He, X. Zhang, S. Ren, and J. Sun, "Deep residual learning for image recognition," *arXiv:1512.03385 [cs]*, 12 2015, arXiv: 1512.03385. [Online]. Available: http://arxiv.org/abs/1512.03385

[33] I. D. Apostolopoulos and T. A. Mpesiana, "Covid-19: automatic detection from x-ray images utilizing transfer learning with convolutional neural networks," *Physical and engineering sciences in medicine*, vol. 43, no. 2, pp. 635–640, 2020.

[34] N. S. Punn and S. Agarwal, "Automated diagnosis of covid-19 with limited posteroanterior chest x-ray images using fine-tuned deep neural networks," *Applied Intelligence*, vol. 51, no. 5, pp. 2689–2702, 2021.

[35] A. Narin, C. Kaya, and Z. Pamuk, "Automatic detection of coronavirus disease (covid-19) using x-ray images and deep convolutional neural networks," *Pattern Analysis and Applications*, vol. 24, no. 3, pp. 1207–1220, 2021.

[36] S. Wang, B. Kang, J. Ma, X. Zeng, M. Xiao, J. Guo, M. Cai, J. Yang, Y. Li, X. Meng *et al.*, "A deep learning algorithm using ct images to screen for corona virus disease (covid-19)," *European radiology*, vol. 31, no. 8, pp. 6096–6104, 2021.

[37] A. Krizhevsky, I. Sutskever, and G. E. Hinton, "Imagenet classification with deep convolutional neural networks," 2012, pp. 1097–1105.

[38] K. Simonyan and A. Zisserman, "Very deep convolutional networks for large-scale image recognition," *arXiv preprint arXiv:1409.1556*, 2014.

[39] C. Szegedy, V. Vanhoucke, S. Ioffe, J. Shlens, and Z. Wojna, "Rethinking the inception architecture for computer vision," 2016 IEEE Conference on Computer Vision and Pattern Recognition (CVPR). Las Vegas, NV, USA: IEEE, 6 2016, pp. 2818–2826, [Online; accessed 2019-04-03]. [Online]. Available: http://ieeexplore.ieee.org/document/7780677/

[40] M. A. Morid, A. Borjali, and G. Del Fiol, "A scoping review of transfer learning research on medical image analysis using imagenet," *Computers in biology and medicine*, vol. 128, p. 104115, 2021.

[41] T. Ozturk, M. Talo, E. A. Yildirim, U. B. Baloglu, O. Yildirim, and U. Rajendra Acharya, "Automated detection of covid-19 cases using deep neural networks with x-ray images," *Computers in Biology and Medicine*, vol. 121, p. 103792, 6 2020.

[42] P. Afshar, S. Heidarian, F. Naderkhani, A. Oikonomou, K. N. Plataniotis, and A. Mohammadi, "Covid-caps: A capsule network-based framework for identification of covid-19 cases from x-ray images," *Pattern Recognition Letters*, vol. 138, pp. 638–643, 2020.

[43] S. Karakanis and G. Leontidis, "Lightweight deep learning models for detecting covid-19 from chest x-ray images," *Computers in biology and medicine*, vol. 130, p. 104181, 2021.

[44] A. Abbas, M. M. Abdelsamea, and M. M. Gaber, "Classification of covid-19 in chest x-ray images using detrac deep convolutional neural network," *Applied Intelligence*, vol. 51, no. 2, pp. 854–864, 2021.

[45] F. M. Salman, S. S. Abu-Naser, E. Alajrami, B. S. Abu-Nasser, and B. A. Alashqar, "Covid-19 detection using artificial intelligence," 2020.

[46] V. Buhrmester, D. Mnch, and M. Arens, "Analysis of explainers of black box deep neural networks for computer vision: A survey," *arXiv:1911.12116 [cs]*, 11 2019, arXiv: 1911.12116. [Online]. Available: http://arxiv.org/abs/1911.12116

[47] E. Zihni, V. I. Madai, M. Livne, I. Galinovic, A. A. Khalil, J. B. Fiebach, and D. Frey, "Opening the black box of artificial intelligence for clinical decision support: A study predicting stroke outcome," *PLOS ONE*, vol. 15, no. 4, p. e0231166, 4 2020, publisher: Public Library of Science.

[48] J. Adebayo, J. Gilmer, M. Muelly, I. Goodfellow, M. Hardt, and B. Kim, "Sanity checks for saliency maps," *arXiv preprint arXiv:1810.03292*, 2018.

[49] B. Zhou, A. Khosla, A. Lapedriza, A. Oliva, and A. Torralba, "Learning deep features for discriminative localization," 2016 IEEE Conference on Computer Vision and Pattern Recognition (CVPR). Las Vegas, NV, USA: IEEE, 6 2016, pp. 2921–2929, [Online; accessed 2019-05-11]. [Online]. Available: http://ieeexplore.ieee.org/document/7780688/

[50] R. R. Selvaraju, M. Cogswell, A. Das, R. Vedantam, D. Parikh, and D. Batra, "Grad-cam: Visual explanations from deep networks via gradient-based localization," *arXiv:1610.02391 [cs]*, 10 2016, arXiv: 1610.02391. [Online]. Available: http://arxiv.org/abs/1610.02391

[51] K. Simonyan, A. Vedaldi, and A. Zisserman, "Deep inside convolutional networks: Visualising image classification models and saliency maps," *arXiv:1312.6034 [cs]*, 12 2013, arXiv: 1312.6034. [Online]. Available: http://arxiv.org/abs/1312.6034

[52] O. Ronneberger, P. Fischer, and T. Brox, "U-net: Convolutional networks for biomedical image segmentation," 2015, pp. 234–241.

[53] S. Arora, A. Risteski, and Y. Zhang, "Theoretical limitations of encoder-decoder gan architectures," *arXiv preprint arXiv:1711.02651*, 2017.

[54] Y. Sugawara, S. Shiota, and H. Kiya, "Super-resolution using convolutional neural networks without any checkerboard artifacts," *arXiv:1806.02658 [cs]*, 6 2018, arXiv: 1806.02658. [Online]. Available: http://arxiv.org/abs/1806.02658

[55] A. L. Maas, A. Y. Hannun, A. Y. Ng *et al.*, "Rectifier nonlinearities improve neural network acoustic models," in *Proc. icml*, vol. 30, no. 1. Citeseer, 2013, p. 3.

[56] J. Antic, *A Deep Learning based project for colorizing and restoring old images (and video!): jantic/DeOldify*, 7 2019, original-date: 2018-10-31T23:32:34Z. [Online]. Available: https://github.com/jantic/DeOldify

[57] J. Lehtinen, J. Munkberg, J. Hasselgren, S. Laine, T. Karras, M. Aittala, and T. Aila, "Noise2noise: Learning image restoration without clean data," *arXiv:1803.04189 [cs, stat]*, 3 2018, arXiv: 1803.04189. [Online]. Available: http://arxiv.org/abs/1803.04189

[58] B. Xu, N. Wang, T. Chen, and M. Li, "Empirical evaluation of rectified activations in convolutional network," *arXiv:1505.00853 [cs, stat]*, 5 2015, arXiv: 1505.00853. [Online]. Available: http://arxiv.org/abs/1505.00853

[59] D. Kermany, K. Zhang, and M. Goldbaum, "Labeled optical coherence tomography (oct) and chest x-ray images for classification," vol. 2, 6 2018, publisher: Mendeley. [Online]. Available: https://data.mendeley.com/datasets/rscbjbr9sj/2

[60] G. Maguolo and L. Nanni, "A critic evaluation of methods for covid-19 automatic detection from x-ray images," *arXiv:2004.12823 [cs, eess]*, 5 2020, arXiv: 2004.12823. [Online]. Available: http://arxiv.org/abs/2004.12823

[61] E. Tartaglione, C. A. Barbano, C. Berzovini, M. Calandri, and M. Grangetto, "Unveiling covid-19 from chest x-ray with deep learning: a hurdles race with small data," *arXiv:2004.05405 [cs, eess]*, 4 2020, arXiv: 2004.05405. [Online]. Available: http://arxiv.org/abs/2004.05405

[62] J. P. Cohen, P. Morrison, and L. Dao, "Covid-19 image data collection," *arXiv 2003.11597*, 2020. [Online]. Available: https://github.com/ieee8023/covid-chestxray-dataset

[63] J. P. Cohen, P. Morrison, L. Dao, K. Roth, T. Q. Duong, and M. Ghassemi, "Covid-19 image data collection: Prospective predictions are the future," *arXiv 2006.11988*, 2020. [Online]. Available: https://github.com/ieee8023/covid-chestxray-dataset

[64] *v7labs/covid-19-xray-dataset*. V7, 9 2020, original-date: 2020-06-17T19:45:19Z. [Online]. Available: https://github.com/v7labs/covid-19-xray-dataset

[65] J. Howard and S. Gugger, "Fastai: a layered api for deep learning," *Information*, vol. 11, no. 2, p. 108, 2020.

[66] L. N. Smith and N. Topin, "Super-convergence: Very fast training of neural networks using large learning rates," in *Artificial intelligence and machine learning for multi-domain operations applications*, vol. 11006. SPIE, 2019, pp. 369–386.

[67] A. S. Musallam, A. S. Sherif, and M. K. Hussein, "Efficient framework for detecting covid-19 and pneumonia from chest x-ray using deep convolutional network," *Egyptian Informatics Journal*, 2022.

[68] M. Abd Elaziz, A. Dahou, N. A. Alsaleh, A. H. Elsheikh, A. I. Saba, and M. Ahmadein, "Boosting covid-19 image classification using mobilenetv3 and aquila optimizer algorithm," *Entropy*, vol. 23, no. 11, p. 1383, 2021.

[69] M. H. Naviwala and R. Qureshi, "Performance analysis of deep learning frameworks for covid 19 detection," in *2021 International Conference on Digital Futures and Transformative Technologies (ICoDT2)*. IEEE, 2021, pp. 1–6.

[70] S. Minaee, R. Kafieh, M. Sonka, S. Yazdani, and G. J. Soufi, "Deep-covid: Predicting covid-19 from chest x-ray images using deep transfer learning," *Medical image analysis*, vol. 65, p. 101794, 2020.

[71] T. Hu, M. Khishe, M. Mohammadi, G.-R. Parvizi, S. H. T. Karim, and T. A. Rashid, "Real-time covid-19 diagnosis from x-ray images using deep cnn and extreme learning machines stabilized by chimp optimization algorithm," *Biomedical Signal Processing and Control*, vol. 68, p. 102764, 2021.

[72] I. M. Baltruschat, L. Steinmeister, H. Ittrich, G. Adam, H. Nickisch, A. Saalbach, J. von Berg, M. Grass, and T. Knopp, "When does bone suppression and lung field segmentation improve chest x-ray disease classification?" in *2019 IEEE 16th International Symposium on Biomedical Imaging (ISBI 2019)*. IEEE, 2019, pp. 1362–1366.

[73] L. O. Teixeira, R. M. Pereira, D. Bertolini, L. S. Oliveira, L. Nanni, G. D. Cavalcanti, and Y. M. Costa, "Impact of lung segmentation on the diagnosis and explanation of covid-19 in chest x-ray images," *Sensors*, vol. 21, no. 21, p. 7116, 2021.

[74] J. Cleverley, J. Piper, and M. M. Jones, "The role of chest radiography in confirming covid-19 pneumonia," *BMJ*, vol. 370, 7 2020, publisher: British Medical Journal Publishing Group section: Practice PMID: 32675083. [Online]. Available: https://www.bmj.com/content/370/bmj.m2426

**Xin Zhang** Xin Zhang is associate researcher in Manchester Metropolitan University (MMU), he received the B.S degree from The PLA Academy of Communication and Commanding, China, in 2009 and Ph.D. degree in Cartography and Geographic Information System from Beijing Normal University(BNU), China, in 2014. His current research interests include remote sensing image processing and deep learning.

**Liangxiu Han** received the Ph.D. degree in computer science from Fudan University, Shanghai, China, in 2002. She is currently a Professor of computer science with the School of Computing, Mathematics, and Digital Technology, Manchester Metropolitan University. Her research areas mainly lie in the development of novel big data analytics and development of novel intelligent architectures that facilitates big data analytics (e.g., parallel and distributed computing, Cloud/Service-oriented computing/data intensive computing) as well as applications in different domains using various large datasets (biomedical images, environmental sensor, network traffic data, web documents, etc.). She is currently a Principal Investigator or Co-PI on a number of research projects in the research areas mentioned above.

**Tam Sobeih** Tam Sobeih is a Research Associate with the School of Computing, Mathematics, and Digital Technology at Manchester Metropolitan University. His interests lie in providing real world solutions to complex problems, through the development of novel intelligent architectures, big data analytics and artificial intelligence applications, leveraging his prior experience in industry.

**Lianghao Han** Dr Lianghao Han received his PhD in Engineering from University of Cambridge (UK) in 2005. He was Professor of Biomedical Engineering in the Medical School at Tongji University (P.R.China) and is a Senior Research Fellow at the Department of Computer Science, Brunel University London. His research focuses on Medical Image Analysis, Machine Learning and Deep Learning for Healthcare.

**Nina Dempsey** Nina Dempsey received her Ph.D. in cancer cell biology from the University of Liverpool in 2009. She is currently a Senior Lecturer in Haematology & Transfusion Medicine at Manchester Metropolitan University in the Department of Life Sciences. Her research interests focus on the identification of biomarkers in critically ill patients and the development of diagnostic tests for use in the Intensive Care Unit.

**Ascanio Tridente** Ascanio Tridente, MD, Ph.D, is a consultant intensivist and physician, the Clinical Director of Critical Care and the chair of Research, Development and Innovation at St Helens and Knowsley Teaching Hospitals NHS Trust. His research interests include sepsis, COVID-19, ARDS, sensors.

**Daoqiang Zhang** received the B.Sc. and Ph.D. degrees in computer science from Nanjing University of Aeronautics and Astronautics, Nanjing, China, in 1999 and 2004, respectively. He is currently a Professor in the Department of Computer Science and Engineering, Nanjing University of Aeronautics and Astronautics. His current research interests include machine learning, pattern recognition, and biomedical image analysis. In these areas, he has authored or coauthored more than 100 technical papers in the refereed international journals and conference proceedings.
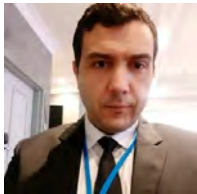
**Symeon Lechareas** Symeon Lechareas is a consultant Vascular and Interventional radiologist working in Whiston and Royal Liverpool University Hospitals. He has research interests in complex peripheral arterial disease and image processing of medical images. He received his Ph.D from University of Athens medical school in 2016 and is currently involved in various research projects.

**Haoming Chen** Haoming Chen is studying for a masters degree in Computer Science and Artificial Intelligence in University of Sheffield. His current research interests include machine learning and Artificial Intelligence.
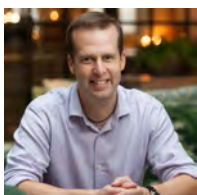
**Stephen White** Stephen White is a cardiovascular biologist with specific interest in vascular pathology. He is a Reader in Cardiovascular Pathology at Manchester Metropolitan University. His work on the underlying triggers of heart attacks focusses on using patient-derived data to understand the molecular processes involved in human disease.